Water Practice & Technology

IWA PUBLISHING

Water Practice & Technology Vol 17 No 10, 2125 doi: 10.2166/wpt.2022.119

Isolated pressure zones based on GIS as a solution for water network problems

Kian Hariri Asli [a,*] and Kaveh Hariri Asli [b]

[a] Department of Electrical and Computer Engineering, Islamic Azad University Tehran North Branch, Tehran, Iran
[b] Department of Mechanical Engineering, Islamic Azad University Rasht Branch, Rasht, Iran
*Corresponding author. E-mail: hariri_k@yahoo.com

KHA, 0000-0001-9495-2712; KHA, 0000-0003-3139-0788

ABSTRACT

One of the most important accidents for water transmission lines occur by air entrance due to water hammer into the water pipeline at sub-atmospheric transient pressure. The air can be sucked into the water system causing repeated pipe breaks in sub-atmospheric transient pressure. This work aimed to improve the advanced techniques including remote sensing (RS), and the internet of things (IoT) to control the repeated pipe breaks. According to the geospatial information systems (GIS), the relationship classes between the spatial and non-spatial data were defined for the scaled model. By GIS the location of pipe breaks and sucking air into water pipeline was recognized during fluid instabilities. The location of pipe breaks was defined by the numerical modelling based on GIS. According to numerical analysis, the Courant number was equal to 0.977. In the field test, the surge velocity was 1084 m/s. The pressure wave was detected in 0.005 s by RS facilities equipped with water hammer sensors, advanced modems, and data loggers referring to the IoT technique. The result of this work led to a reduction of the non-revenue water (NRW) and the saving of drinking water.

Key words: geospatial information systems, internet of things, non-revenue water, remote sensing, water hammer, water transmission

HIGHLIGHTS

- Connection between GIS, RS, and IoT for record the water pressure wave (in this work 0.005 s).
- Conceptual modeling definition for prediction of the pressure wave variation due to water hammer.
- Improvement of RS facilities installation equipped with data loggers, IoT and GEO-database.
- Relationship class definition for water system elements for leakage points.
- Make water and energy savings.

GRAPHICAL ABSTRACT

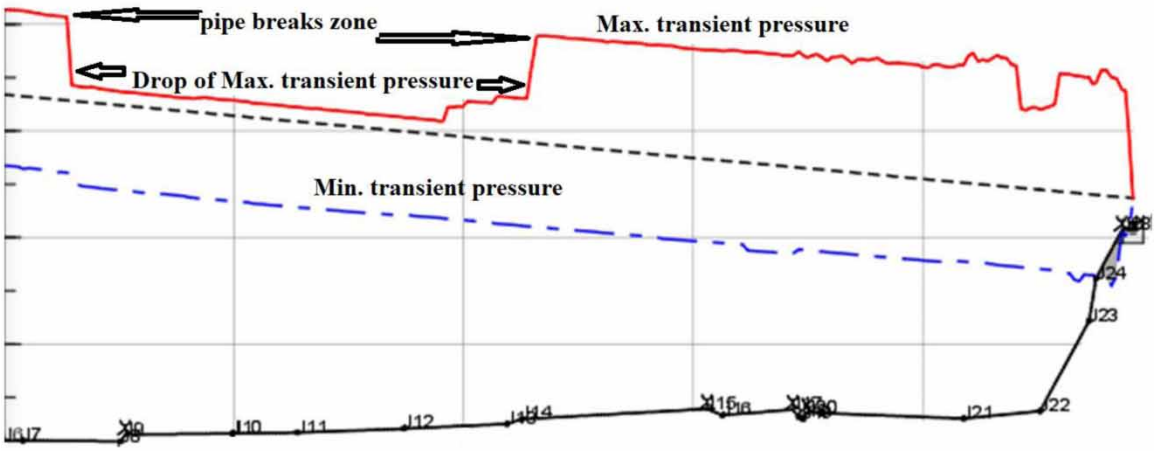

ABBREVIATIONS

d	Outer diameter of the pipe (m)
δ	Wall thickness (mm)
V_0	Average speed of water (m/s)
t	Time (S)
V	Volume (m^3)
τ	Shear stress
γ	Specific weight (N/m^3)
A	Pipe cross-sectional area (m^2)
P	Surge pressure (Pa)
W	Weight of fluid element (Kg)
θ	Angle of fluid element with X direction
$k = \frac{d\rho}{\frac{d\rho}{\rho}}$	(fluid module of elasticity)
g	Acceleration of gravity (m/s^2)
f	Friction
t	Time (S)
γ	Fluid-specific weight
λ_0	Unit of a length
V	Velocity of fluid element (m/s)
S	Length (m)
d	Diameter of pipe (mm)
π	Mathematical constant, approximately equal to 3.14159.
Δv	Velocity deference of fluid $kg/m.s$
h_p	Head gain from a pump (m)
h_L	Combined head loss (m)
C	Velocity of surge wave (m/s)
P/γ	Pressure head (m)
Z	Elevation head (m)
$V^2/2g$	Velocity head (m)
γ	Fluid specific weight (N/m^3)
Z	Elevation (m)
H_P	Surge wave head at intersection points of characteristic lines (m)
V_P	Surge wave velocity at pipeline points – intersection points of the characteristic lines (m/s)
V_{ri}	Surge wave velocity at right-hand side of the intersection points of the characteristic lines (m/s)
H_{ri}	Surge wave head at right hand side of the intersection points of characteristic lines (m)
V_{le}	Surge wave velocity at the left-hand side of intersection points of characteristic lines (m/s)
H_{le}	Surge wave head at the left-hand side of intersection points of characteristic lines (m)
p	Pressure (bar), (N/m^2)
dV	Incremental change in liquid volume with concerning to the initial volume
$(d\rho/\rho)$	Incremental change in liquid density concerning to initial density
a	Velocity of surge wave (m/s)
ρ	Density of water (kg/m^3)
E_W	Modulus of elasticity of the water, $E_W = 2 \cdot 10^9 Pa$, (kg/m^2)
D	Diameter of pipe (mm)
E	Modulus of elasticity for pipeline material Steel, $E = 10^{11} Pa$, (kg/m^2)
P	Pressure of the water (bar), (N/m^2)
n	Percent of air volume (m^3)
t_W	Wall thickness of the pipe (mm)
g	Acceleration of gravity (m/s^2)
h	Head of the liquid (water) column(m)

SUPERSCRIPTS

C^-	Characteristic lines with a negative slope
C^+	Characteristic lines with a positive slope

SUBSCRIPTS

Min.	Minimum
Max.	Maximum

Lab.	Laboratory
MOC	Method of characteristic
GIS	Geospatial information system
PLC	Program logic control
NRW	Non-revenue water
FD	Finite differences
WCM	Wave characteristic method
FE	Finite elements
FV	Finite volume
IoT	Internet of things
RS	Remote sensing
SRV	Surge relieve valve
FSI	Fluid-structure interaction

1. INTRODUCTION

Fluid-structure interaction (FSI) in pipe systems is defined as the transfer of momentum and forces in both ways, between the pipe wall and the contained fluid during unsteady flow (Andrade & de Freitas Rachid 2022). The fluid hammer taking place here not only leads to high-pressure peaks in the fluid but also to low pressures, During the fluid hammer compression wave, the pressure evolution is accompanied by a complex multiphase flow pattern. First of all, a foamy mixture of non-condensable gas, vapour, and liquid droplets precedes the liquid front arrival at the bottom end, the vapour condensates and the non-condensable gas gets compressed. Afterward, the arrival of an expansion wave induces the movement of the liquid column backward, with the corresponding pressure drop that generates a gaseous bubble, referred to as column separation. Finally, the collapse of this bubble is at the origin of the next pressure rise (Ferras *et al.* 2018). Various methods have been developed to solve transient flow in pipes. Much research has been carried out on the optimization of water distribution systems (WDSs). Within the last decade, the focus has shifted from the use of traditional optimization methods, such as linear and nonlinear programming, to the use of heuristics derived from nature (HDNs), namely, genetic algorithms, simulated annealing, and more recently, ant colony optimization (ACO) as an optimization algorithm based on the foraging behaviour of ants (Hariri Asli & Nazari 2021). The approaches proposed to solve the single-phase pure liquid water hammer equations are the method of characteristics (MOC), finite differences (FD), wave characteristic method (WCM), finite elements (FE), and finite volume (FV). Many researchers have made significant contributions in this area. Some of them popularized the graphical method of calculation. They also developed various methods of investigation of water age and leakage in water systems (Hariri Asli & Hozori 2021). Generally, the hydraulic transient pressure happened by massive outflow due to the pipeline's local breaks. The power turning on and off led to stopping the pump and the water hammer attacking the system. In power turning on and off cases the equipment which can help during an emergency outage includes a surge tank, pressure relief valves, pressure vessels for the pulse pressure damping, pressure reducing valves, pressure relief valves, and air relief valves. According to the dependence of the water hammer on the profile of the water transmission line, it is necessary to run research for checking extreme transient pressures in the water system by GEO-database intercommunication and geospatial information systems (GIS). For the long pipeline with large diameters and initial velocities in excessive variations in elevation, it is a good idea to check the extreme transient pressures for the systems due to GEO-referenced coordination. Some researchers defined the hydraulic model for non-revenue water (NRW) based on the GIS. They saved the drinking water with a 3D hierarchical model equipped with remote sensing (RS) facilities (Hariri Asli 2022). The differences of the present work against previous investigations are as follows:

- Investigation of the bubbles sucked into the system in low transient time (up to 5 milliseconds).
- Investigation of the pressure wave velocity in low transient time (up to 5 milliseconds).
- Improve the advanced techniques including RS, and the internet of things IoT (IoT) to control the repeated pipe breaks.

Referring to the presented background, the aims of the present work include the hydraulic model design related to the repeated pipe breaks in the field of sub-atmospheric pressure in compliance with GIS. Hence the spatial and non-spatial data were collected by data loggers incorporated with the IoT and the RS facilities. This combination of techniques helped the control of accidents that happen by air entrance related to the water hammer. This procedure led to the saving of drinking water in the water transmission process.

2. METHODS

The rapid changes in the velocity of water by stopping the second layer of liquid and exerting pressure on the following layers gradually caused transient flow with high wave pressure as long as the water hammer reveals in the water systems. It acts directly at the valves and extends to the rest of the pipeline against fluid flow speed. If the pressure at the beginning of the pipeline remains unchanged then after the shock of the initial section of the pipe, it begins the reverse movement of the shock wave with the same velocity. Among the various methods for investigation of transient flow, the MOC combined with computer modeling and subject to transient flow is still growing fast around the world. In this work, a case with outflow due to local breaks with the possibility of sucking air in the negative phase into the pipeline was investigated for two scenarios:

- First, case of transmission line equipped with a surge tank.
- Second, case of transmission line not equipped with a surge tank.

2.1. Formulation

The conservation equations of mass, momentum, and energy for the constituents can be obtained by using the classical approach of continuum mechanics (Lema *et al.* 2016). For flow in 3D motion, the governing equations are simultaneously solved for liquid and the gas phases and the gas-liquid interface are automatically calculated by the program (Möller *et al.* 2015). The transient theory stems from the two governing equations. The momentum equation and continuity equation are needed to determine velocity and surge pressure in the flow system. The solving of these two equations produces a theoretical result that usually corresponds quite closely to actual system measurements (Equations (1)–(25)) if the data and assumptions used to build the numerical model are valid. The calculation automatically sub-divided the pipe into sections and selected a time interval for computations.

The Euler equation can be regarded as a consequence of the conservation of momentum. The derivation of the Euler equation can be considered an infinitesimal fluid volume with mass. The motion of the fluid element can be described from a fixed coordinate system (Eulerian approach). By definition, the considered fluid element moves along an arbitrarily oriented streamline:

$$\frac{dV}{dt}+\frac{1}{\rho}\cdot\frac{\partial \mathrm{P}}{\partial S}+g\frac{dZ}{dS}+\frac{f}{2D}V|V|=0 \quad \text{(Euler equation)} \tag{1}$$

An infinitesimal volume element, to which a single density, changing over time, can be assigned. In the next step, the size of the infinitesimal element does not matter anyway and thus it can indeed be chosen infinitesimal element does not matter anyway and thus it can indeed be chosen infinitesimally small. Furthermore, note that the density inflows generally vary not only over time but also it changes from one point to another (e.g. in a pipe diameter contraction). The temporal change of density is therefore a partial derivative of the density respect to time. Hence we need to 'conservation of mass' law for finding parameters V and P.

This equation is finally called the continuity equation and is valid in this form for one-dimensional flows. This equation results from the conservation of mass. The continuity equation serves to determine the temporal change of density in arbitrary points of a flow using the existing flow field (represented by the vectors of the mass flux):

$$C^2\frac{\partial V}{\partial S}+\frac{1}{\rho}\cdot\frac{dp}{dt}=\circ \quad \text{(continuity equation)} \tag{2}$$

The partial differential Equations (1) and (2) are solved by the method of characteristics MOC:

$$\frac{dp}{dt}=\frac{\partial p}{\partial t}+\frac{\partial p}{\partial S}\cdot\frac{dS}{dt} \tag{3}$$

$$\frac{dV}{dt}=\frac{\partial V}{dt}+\frac{\partial V}{\partial S}\cdot\frac{dS}{dt} \tag{4}$$

$$\left|\frac{\partial V}{\partial t}+\frac{1}{\rho}\frac{\partial p}{\partial S}+g\frac{dz}{dS}+\frac{f}{2D}V|V|=\circ\right. \tag{5}$$

$$\mathrm{C}^2\frac{\partial V}{\partial S}+\frac{1}{\rho}\frac{\partial P}{\partial t}=\circ \tag{6}$$

$$\lambda\left(\frac{\partial V}{\partial t}+\frac{1}{\rho}\frac{\partial p}{\partial S}+g.\frac{dz}{dS}+\frac{f}{2D}V|V|\right)+c^2\frac{\partial V}{\partial S}+\frac{1}{\rho}\frac{\partial p}{\partial t}=\circ \tag{7}$$

$$\left(\lambda\frac{\partial V}{\partial t}+C^2\frac{\partial V}{\partial S}\right)+\left(\frac{1}{\rho}.\frac{\partial \rho}{\partial t}+\frac{\lambda}{\rho}.\frac{\partial P}{\partial S}\right)+\lambda.g.\frac{dz}{dS}+\frac{\lambda.f}{2D}V|V|=\circ \tag{8}$$

By linear combination of Equations (5) and (6):

$$\lambda\frac{\partial V}{\partial t}+C^2\frac{\partial V}{\partial S}=\lambda\frac{dV}{dt}\Rightarrow\lambda\frac{dS}{dt}=C^2 \tag{9}$$

$$\frac{1}{\rho}.\frac{\partial p}{\partial t}+\frac{\lambda}{\rho}.\frac{\partial \rho}{\partial S}=\frac{1}{\rho}.\frac{d\rho}{dt}\Rightarrow\frac{\lambda}{\rho}=\frac{1}{\rho}.\frac{dS}{dt} \tag{10}$$

$$\left|\frac{C^2}{\lambda}=\lambda\right.$$

(By removing $\frac{dS}{dt}$), $\lambda=\pm C$.

For $\lambda=\pm C$, from Equation (10) we have:

$$C\frac{dV}{dt}+\frac{1}{\rho}.\frac{dp}{dt}+C.g.\frac{dz}{dS}+C.\frac{f}{2D}V|V|=\circ$$

By dividing both sides by 'C':

$$\frac{dV}{dt}+\frac{1}{c.\rho}\frac{dP}{dt}+g.\frac{dz}{dS}+\frac{f}{2D}V|V|=\circ \tag{11}$$

For $\lambda=-C$ by Equation (8):

$$\frac{dV}{dt}-\frac{1}{c.\rho}\frac{dp}{dt}+g.\frac{dz}{dS}+\frac{f}{2D}V|V|=\circ \tag{12}$$

If $\rho=\rho.g(H-Z)$.

From Equations (2) and (3) we have:

$$\left|\frac{dV}{dt}+\frac{g}{c}.\frac{dH}{dt}+\frac{f}{2D}V|V|=\circ\right. \tag{13}$$

$$\left|if:\frac{dS}{dt}=C\right. \tag{14}$$

$$\left|\frac{dV}{dt}-\frac{g}{c}.\frac{dH}{dt}+\frac{f}{2D}V|V|=\circ\right. \tag{15}$$

$$\left|if:\frac{dS}{dt}=-C\right. \tag{16}$$

Equations (14) and (16) are the characteristic Equations of (13) and (15).

If: $f=0$ then Equation (14) will be:

$$\frac{dV}{dt}-\frac{g}{c}.\frac{dH}{dt}=\circ$$

or

$$dH=\frac{C}{g}dV\quad(Zhukousky) \tag{17}$$

If the pressure at the inlet of the pipe and along its length is equal to p_0, then slugging pressure undergoes a sharp increase:

$$\Delta p_{y\partial}: p = p_0 + \Delta p_{y\partial}$$

The Zhukousky formula is as follows:

$$\Delta p_{y\partial} = \left(C \cdot \frac{\Delta v}{g}\right) \tag{18}$$

The speed of the shock wave is calculated by the formula:

$$C = \sqrt{\frac{g \cdot \frac{E_W}{\rho}}{1 + \frac{d}{\delta} \cdot \frac{E_W}{E}}} \tag{19}$$

By finite difference method of water hammer:

$$T_p - 0 = \Delta t$$

$$c^+: \frac{\left(V_P - V_{Le}\right)}{\left(T_P - \circ\right)} + \left(\frac{g}{c}\right)\left(\frac{\left(H_P - H_{Le}\right)}{\left(T_P - \circ\right)}\right) + \left(\frac{fV_{Le}\left|V_{Le}\right|}{2D}\right) = \circ \tag{20}$$

$$c^-: \frac{\left(V_P - V_{Ri}\right)}{(T_P - \circ)} - \left(\frac{g}{c}\right)\left(\frac{(H_P - H_{Ri})}{(T_P - \circ)}\right) + \left(\frac{fV_{Ri}\,|V_{Ri}|}{2D}\right) = \circ \tag{21}$$

$$c^+: (V_P - V_{Le}) + \left(\frac{g}{c}\right)(H_P - H_{Le}) + (f.\Delta t)\left(\frac{V_{Le}|V_{Le}|}{2D}\right) = \circ \tag{22}$$

$$c^-: (V_P - V_{Ri}) - \left(\frac{g}{c}\right)(H_P - H_{Ri}) + (f.\Delta t)\left(\frac{V_{Ri}\,|V_{Ri}|}{2D}\right) = \circ \tag{23}$$

$$V_p = \frac{1}{2}\left[\left(\frac{C}{g}\right)(V_{Le} + V_{Ri}) + \left(\frac{g}{c}\right)(H_{Le} - H_{Ri}) - \frac{f.\Delta t}{2D}(V_{Le}|V_{Le}| + V_{Ri}|V_{Ri}|)\right] \tag{24}$$

$$H_p = \frac{1}{2}\left[\left(\frac{C}{g}\right)(V_{Le} - V_{Ri}) + (H_{Le} + H_{Ri}) - \left(\frac{C}{g}\right)\frac{f.\Delta t}{2D}(V_{Le}|V_{Le}| - V_{Ri}|V_{Ri}|)\right] \tag{25}$$

In the above equations the parameters V_{Le}, V_{Ri}, H_{Le}, H_{Ri}, f and D are the initial conditions. These parameters resulted in the solution at the steady-state conditions. The water hammer equations calculation started with pipe length 'L' division by 'N' parts:

$$\Delta S = \frac{L}{N} \;\&\; \Delta t = \frac{\Delta s}{C}$$

Equations (24) and (25) are solved for P_2 to P_N then H and V are found for internal points.

For P_1, there is only one characteristic line (c^-).

For P_{N+1}, there is only one characteristic line(c^-).

For finding H and V, P_1 and P_{N+1} are used as the boundary conditions.

The challenge of selecting a time step is made difficult in pipeline systems by two conflicting constraints defined by the dynamic model for water hammer. First, to calculate many boundary conditions, such as obtaining the head and discharge at the junction of two or more pipes, the time step must be common to all pipes. The second constraint arises from the nature of the MOC. If the adjective terms in the governing equations are

neglected, the MOC requires that the ratio of the distance x to the time step t be equal to the wave speed in each pipe. In other words, the Courant number should ideally be equal to one and must not exceed one for stability reasons. Faced with this challenge, researchers have sought ways of relaxing the numerical constraints. Two contrasting strategies present themselves. The propagation time calculation of the shock wave due to the water hammer is an important point. The velocity of the water hammer wave in the tube could be obtained by dividing the path length between the two pressure measuring points by the propagation time of the water hammer wave between those two points (Sarkardeh *et al.* 2014).

After shock wave generation, flow moved with the same velocity in the reverse direction of the shock wave. This led to the generation of high-pressure loss due to the wave and fluid moving in the reverse direction of the pipeline. As long as the shock wave reached the pressure-reducing valve, liquid pressure was reduced to vapor pressure. By the way, again and again, the wave of pressure drop moved conversely in the direction of the start point on the water pipeline.

As long as the damping shock wave, these cycles of increased and decreased pressure were continued. It was iterated at time intervals equal to the time for the dual-path of the shock wave along with the length of the pipeline. The shock wave or transient waves are formed during the transient flow states in the urban water supply system (UWSS).

Transient waves are high-speed elastic shocks that travel at relatively high velocities in pipeline systems (e.g., about 1000 m/s in metallic pipes and around 400 m/s in polymeric pipes) (Vardy *et al.* 2015). Transient pressure is associated with a rapidly filling pipeline containing two entrapped air pockets which are investigated experimentally and numerically. A multiple-air-pocket elastic-water model considering multiple moving boundaries of water columns is developed by neglecting inertia and head loss of a short water column near air-water interfaces. This presented an intrinsic approach to estimating air entrainment rates due to intake vortices based on large-scale laboratory measurements. Quasi-continuous measurements of the amount of entrained air were conducted using a sophisticated de-aeration system (Zecchin *et al.* 2005; Zhao *et al.* 2020). The data analysis of experimental runs resulted in a parameter fit describing the air entrainment rates at horizontal intakes.

2.2. Methods

This work focused on the techniques of the advanced methods against water transmission failure due to water hammer. In the present project, at June 2016, the water pipeline was equipped with RS facilities, ultrasonic flow meters (UFMs), pressure sensors and data logger system. The RS in with IoT for rapid data intercommunication were used. Then the leakage points of water pipeline were investigated. Modern technology through advanced water hammer pressure sensors and modems were applied for the detection of a surge pressure wave in accordance with up to 1 second. To reduce the risk of water transmission failure, the relationship classes between the spatial data and non-spatial data as a tool for communication between coordination of water system elements related to GEO-database intercommunication through program logic control (PLC) were defined. The relationship class for water system elements according to the type of connection was linked to the leakage points. The hydraulic model of NRW for analysis of water loss was defined in compliance with GIS. The numerical techniques were used in water hammer analysis based on the HAMMER-ArcGIS-ArcMap software. In this work, the water pipeline was recognized by numerical analysis such as the finite difference method (FDM) based on the GIS.

Today, the vast map information and the need to update it in the form of a dynamic system has put the use of GIS on the agenda planners. A strong data base can be the solution to many problems. If map information is only stored in the memory of experts, it can be easily removed from the system with the passage of time. Therefore, it is necessary to create an information data base to make the best decisions and apply management in the shortest possible time. The correct use of resources and intelligent management is possible through the use of new technologies such as GIS, production and exchange of experiences and technical work knowledge. For this reason, GIS and location intelligence applications are at the foundation of location-enabled services, which rely on geographic analysis and visualization.

This key characteristic of GIS has begun to open new avenues of scientific inquiry and studies.

Achievements of utilization by GIS for the water industry are as follows:

- Scientific management through the analysis of data received from sensors related to various hydraulic parameters such as pressure, flow rate water by RS.

- Identifying any qualitative and quantitative changes in the set of facilities.
- ON- LINE management of water facilities while using remote reading technique according to GIS.
- Creating a GEO-database and tracking and implementing network analysis to control water losses.
- Creation of GEO-referenced maps and to provide systematic reporting.
- Record the water facility equipment GEO-database by using GIS.
- Combination of the above analyzes for optimal management of water facilities.

2.3. Research apparatus

The experimental system was composed of an upstream water reservoir (Res.1 in Figure 1), downstream water reservoir (Res.2 in Figure 1), pump station, pipeline, pressure relief valve, pressure gauges, UFMs, pressure sensors, remote sensing, data logger system, and an open-end surge tank placed on the discharge side of a pump station as a device for the control of both positive and negative surges. This hydro-pneumatic tank is a relatively small pressurized vessel, containing both air and liquid, which is connected to the discharge line from the pump station. The primary purpose of the air chamber is to prevent negative pressures and column separation in the pipeline downstream of the pump station during power failure rundown. However, the device can be a positive surge suppresser as well. In this work, the surge tank (Figure 1) with a volume of 6 cubic meters was equipped with a 350 mm diameter surge relieve valve (SRV) and an air chamber safety valve. As shown in Figure 1, the water delivery system pumps water from the upstream water reservoir to the downstream water reservoir. The layout of the present work includes a water transmission line, suction and discharge reservoirs, a project line of the piping, and the natural ground level (Figure 1).

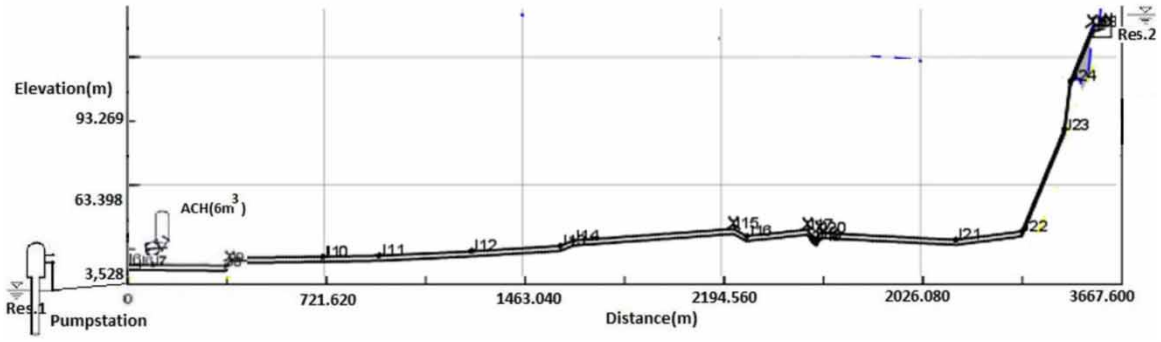

Figure 1 | Layout of water transmission line and pump station, surge tank, leakage location, suction and discharge reservoirs.

2.4. Hydraulic model and the apparatus

The definition process of the hydraulic model due to water hammer in compliance with GIS needs to apply the advanced techniques including RS, data loggers with modems, and IoT. These techniques can be classified based on the type of facilities for detection of spatial and non-spatial data and data intercommunication through GSM, GPRS, and SMS. The apparatus for the present work can be itemized by the following cases:

- GIS.
- HAMMER-ArcGIS-ArcMap software for water hammer analysis.
- RS facility equipped with modems and data loggers.
- IoT as modern technology for rapid data intercommunication.
- GEO-database intercommunication by RS against water transmission failure due to water hammer.

The hydraulic impact of the liquid in the pipeline performed oscillatory motion. The hydraulic model (Table 1) against shock waves for the present work includes a one-way surge tank for protection of the water transmission line against water hammer. Hence, the flow and pressure sensors equipped with data loggers were installed into the manholes of valves along the water transmission line. The flow and pressure variation due to water hammer were detected by sensors and transmitted by modems to the RS. These collected data were instantaneously compared with the calibrated mathematical model of the pipeline. The online comparison between the spatial data

Table 1 | Specification of hydraulic model of water transmission line

	Keyword	Value
1	Units for flow	M^3/s
2	Units for head	m
3	Units for volume	m^3
4	Units for diameter	mm
5	Units for length	m
6	Units for mass	kg
7	Time increment	0.0148
8	Number of time steps	339
9	Simulation time	5.003 (s)
10	Wave speed	1084 (m/s)
11	Vapor pressure	−10 (bar)
12	Max. volume	198.483 (m^3)
13	Type of volume	Air
14	Type	air valve
15	Category	Protection equip
16	Node ID	24
17	Label	J28
18	Units for pressure	mH
19	Specific gravity	1
20	Courant number	Cr = 0.997

and non-spatial data made a communication between coordination of water system elements related to the GEO-database of the pipeline which revealed the water leakage zones in the present work (Asli *et al.* 2012, 2017; Duan *et al.* 2020).

2.5. Calibration of the apparatus

Calibration of the apparatus includes the instruments and meters carried out by RS facilities equipped with modems and data loggers. The pressure sensors were employed in the experiments. According to the measurement principle and instructions, the physical quantities measured by the UFM and pressure sensors were linearly related to the output and the signals were calibrated in a steady state. The UFM was calibrated before it leaves the factory; therefore, we needed only to check that the UFM head pressure was consistent with the stored value in laboratory tests to ensure the correctness of transmission. The pressure sensors were calibrated by using a pressure gauge, and a check also needs to be performed to ensure that the pressure sensors are consistent with the stored value in laboratory tests. The PLC controlled the valve closing speed by adjusting the speed of the actuator motor for control valves. The closing time for control valves was recorded in laboratory tests.

A UFM is a type of flowmeter that measures the velocity of a fluid with ultrasound to calculate volume flow. Using ultrasonic transducers, the flow meter can measure the average velocity along the path of an emitted beam of ultrasound, by averaging the difference in measured transit time between the pulses of ultrasound propagating into and against the direction of the flow or by measuring the frequency shift from the Doppler effect. Ultrasonic flowmeters are affected by the acoustic properties of the fluid and can be impacted by temperature, density, viscosity and suspended particulates depending on the exact flowmeter. They have the following distinguishing advantages:

- Flow measurements in large pipes can be carried out.
- Flow of both gases and liquids can be measured.
- Ultrasonic flowmeters can measure the flow of nonconductive flows.
- For the measurement of low flow rates, the ultrasonic flowmeter is a better option compared to the Vortex flowmeter.
- They have no moving parts, so there are no wear and tear issues.

3. RESULTS AND DISCUSSION

In this work, the nominal diameter of the water pipeline was 1250 mm and the water flow rate was 3 cubic meters per second.

The water velocity in the pipe was 2.44 m/s and the water hammer wave speed was 1084 (m/s). The upstream reservoir ground level was 40.95 m and the downstream reservoir ground level was 103.50 m. The water transmission failure happened in the field of sub-atmospheric transient pressures. The air influence (Tables 2 and 3) on hydraulic modeling with two different types of air content models were proposed in predicting the transient pressure behavior by HAMMER-ArcGIS-ArcMap software analysis and water pipeline leakage detection process (Figures 2 and 3).

Table 2 | Vapor bubbles due to air infiltration into water pipeline

Type of point	Percent of air volume (cm)
P10	92.31
P11	95.24
P12	95.24
P13	66.67
P14	97.30
P14:J15	Air
P15	66.67
P15:J15	Air
P16	92.86
P16:J17	Air
P17:J17	Air
P19:J20	Air
P20	96.77
P20:J20	Air
P21	93.75
P22	90.00
P23	50.00
P24	80.00
P24:J28	Air
P25	66.67
P25:J28	Air
P3	95.00
P5:J26	Air
P6	85.71
P6:J26	Air
P7	50.00

This process included the concentrated vaporous cavity model and the discrete air release model (Tables 2 and 3). By regression analysis and through investigation of Scatter diagram and the curve fit due to regression analysis, surge velocity against the volume of sucked air into the transmission line (Equations (26) and (27)) showed a good correlation between the dependent variable (surge velocity) and the independent variable (volume of sucked air) data (Figures 3 and 4). The results of a modeled air entrainment in real prototype systems showed the maximum volume (198.483 m^3) of infiltrated air (Figures 4–6). The surge tank was located at point P2: J4 and the maximum amount of infiltrated air at point P24: J28 was equal to 198.483 m^3 (Table 3). In this condition the vapor pressure was equal to −10 bar.

Table 3 | The modeling of the pipeline by ArcGIS-ArcMap and HAMMER software

Node ID	Label	Category	Vapor pressure (bar)	Max. volume (m^3)	Type of volume
1	J2	Junction	−10	0	Vapor
2	J4	Surge tank	−10	0	Vapor
3	J1	Reservoir	−10	0	Vapor
4	J3	Pump	−10	0	Vapor
5	J7	Junction	−10	0	Vapor
6	J8	Junction	−10	0	Vapor
7	J11	Junction	−10	0	Vapor
8	J12	Junction	−10	0	Vapor
9	J14	Junction	−10	0	Vapor
10	J16	Junction	−10	0	Vapor
11	J18	Junction	−10	0	Vapor
12	J19	Junction	−10	0	Vapor
13	J21	Junction	−10	0	Vapor
14	J22	Junction	−10	0	Vapor
15	J23	Junction	−10	0	Vapor
16	J27	Junction	−10	0	Vapor
17	J26	Prot equip	−10	0	Air
18	J9	Prot equip	−10	0	Air
19	J10	Junction	−10	0	Vapor
20	J15	Prot equip	−10	0	Air
21	J17	Prot equip	−10	0	Air
22	J20	Prot equip	−10	0	Air
23	J24	Junction	−10	0	Vapor
24	J28	Prot equip	−10	198.483	Air
25	N1	Reservoir	−10	0	Vapor
26	J6	Junction	−10	0	Vapor
27	J13	Junction	−10	0	Vapor

The *p*-value is the level of marginal significance within a statistical hypothesis test representing the probability of the occurrence of a given event. The *p*-value is used as an alternative to rejection points to provide the smallest level of significance at which the null hypothesis would be rejected. In this work, the following procedure was carried out for the *p*-value evaluation:

- Determine the experiment's expected results.
- Determine the experiment's observed results.
- Determine the experiment's degrees of freedom.
- Compare expected results to observed results with chi-square.
- Choose a significance level.
- Use a chi-square distribution table to approximate the *p*-value.
- Approximate *p*-value for an experiment, it can be decided whether or not to reject the null hypothesis of the experiment.

Generally, based on the hypothesis and the experimental results, if the *p*-value is lower than the significance value, it can be shown that the experimental results would be highly unlikely to occur if there was no acceptable relation between the variables which are manipulated (Table 4).

In this work, the *p*-values for two variables (surge velocity; the volume of sucked air into the transmission line) are as follows (Table 4):

(1) *p*-value for surge velocity (m/s):

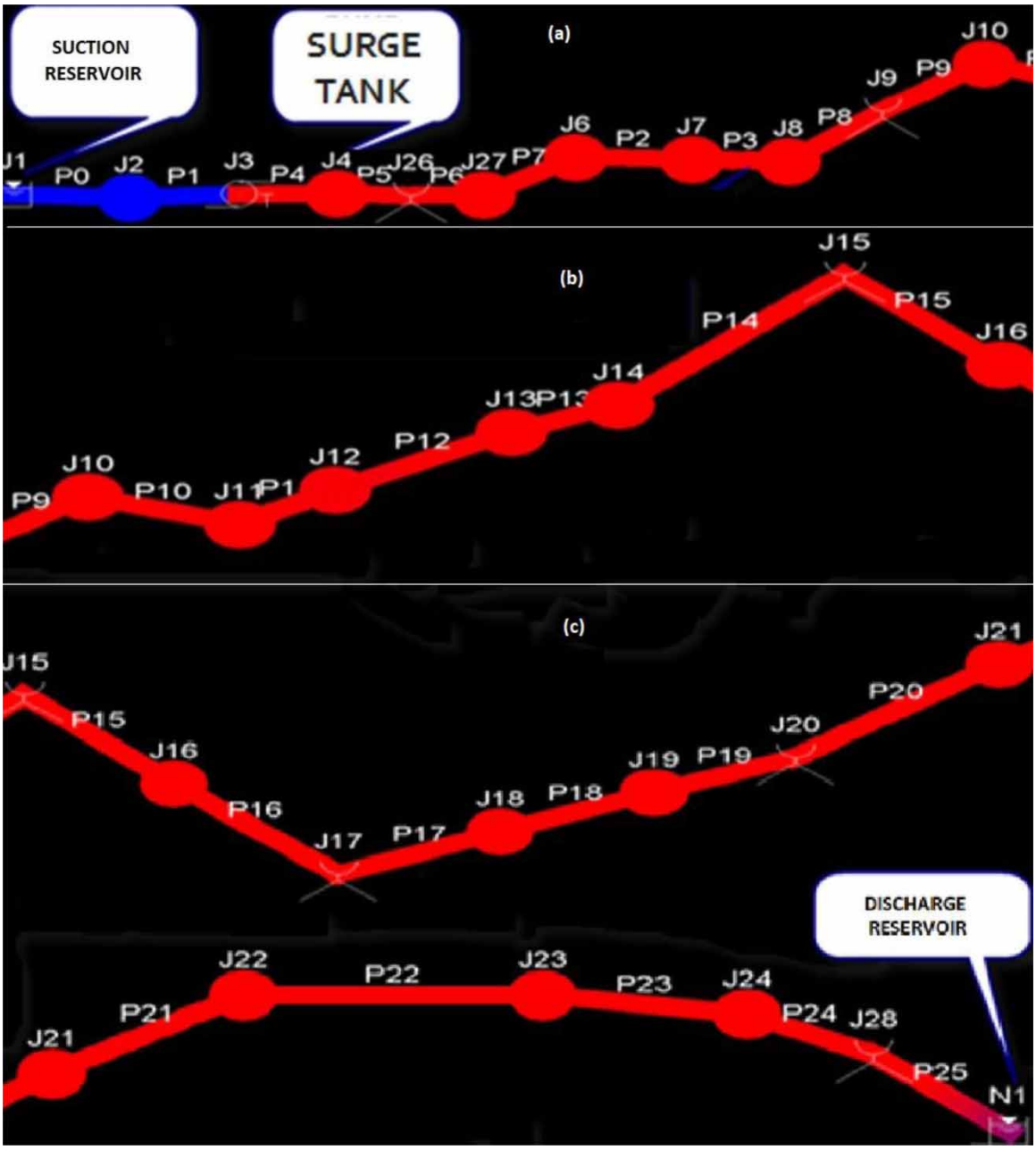

Figure 2 | water hammer analysis of water pipeline (HAMMER & ArcGIS-ArcMap software); (a) First pressure zone, (b) Second pressure zone, (c) Third pressure zone.

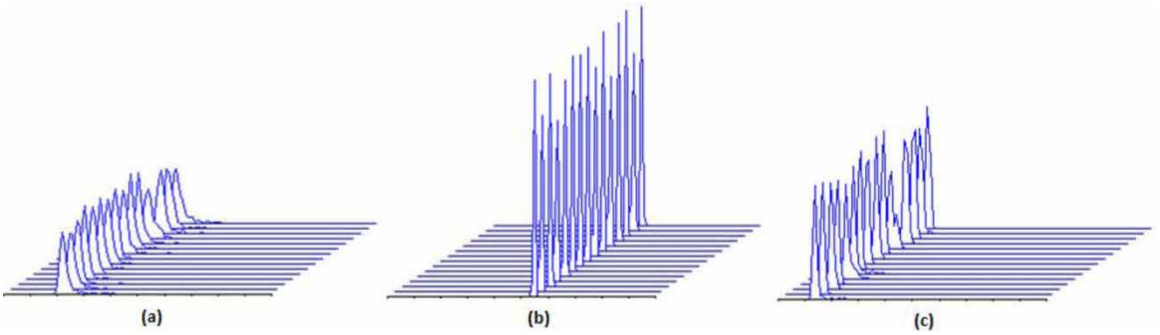

Figure 3 | Leakage location at water transmission line (Leakage detection range: (0–100 dB); (a) before transition pressure pulse perturbations, (b) at transition pressure pulse perturbations, (c) after transition pressure pulse perturbations.

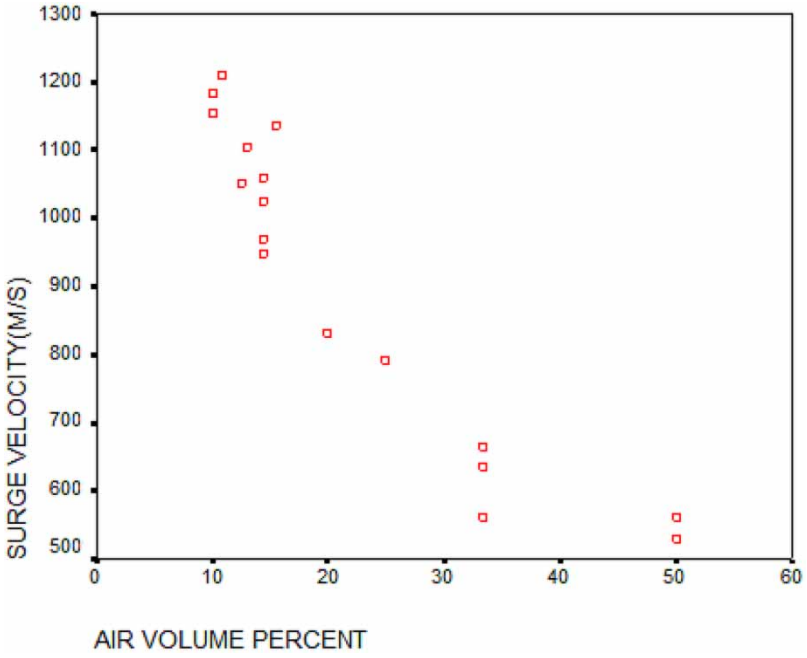

Figure 4 | Scatter diagram due to regression analysis; surge velocity against the volume of sucked air into the transmission line.

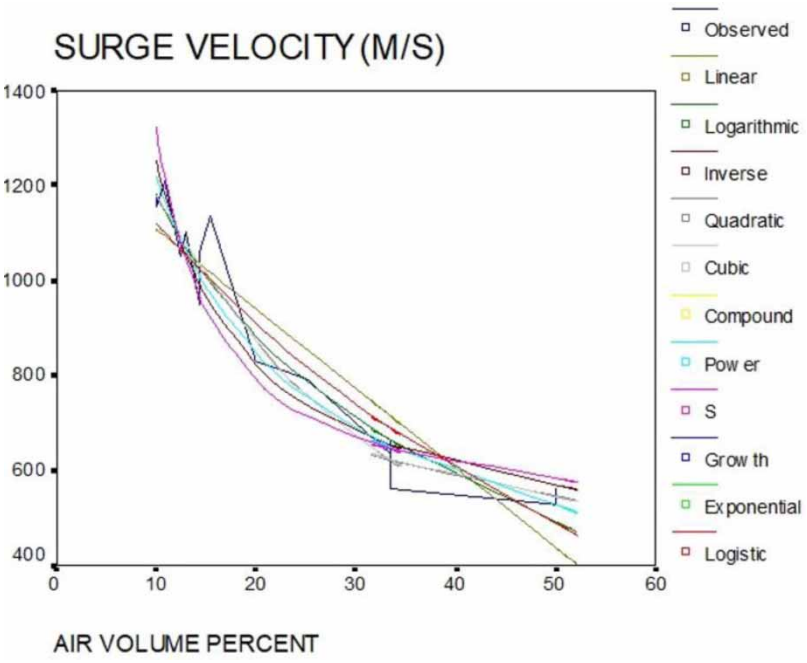

Figure 5 | Curve fit due to regression analysis; surge velocity against the volume of sucked air into the transmission line.

Chi 2 = 1.200, DF = 7
The *p*-value equals 0.991.
By conventional criteria, this difference is considered to be not statistically significant.

(2) *p*-value for air volume (%):

Chi 2 = 1.200, DF = 6
The *p* value equals 0.977.

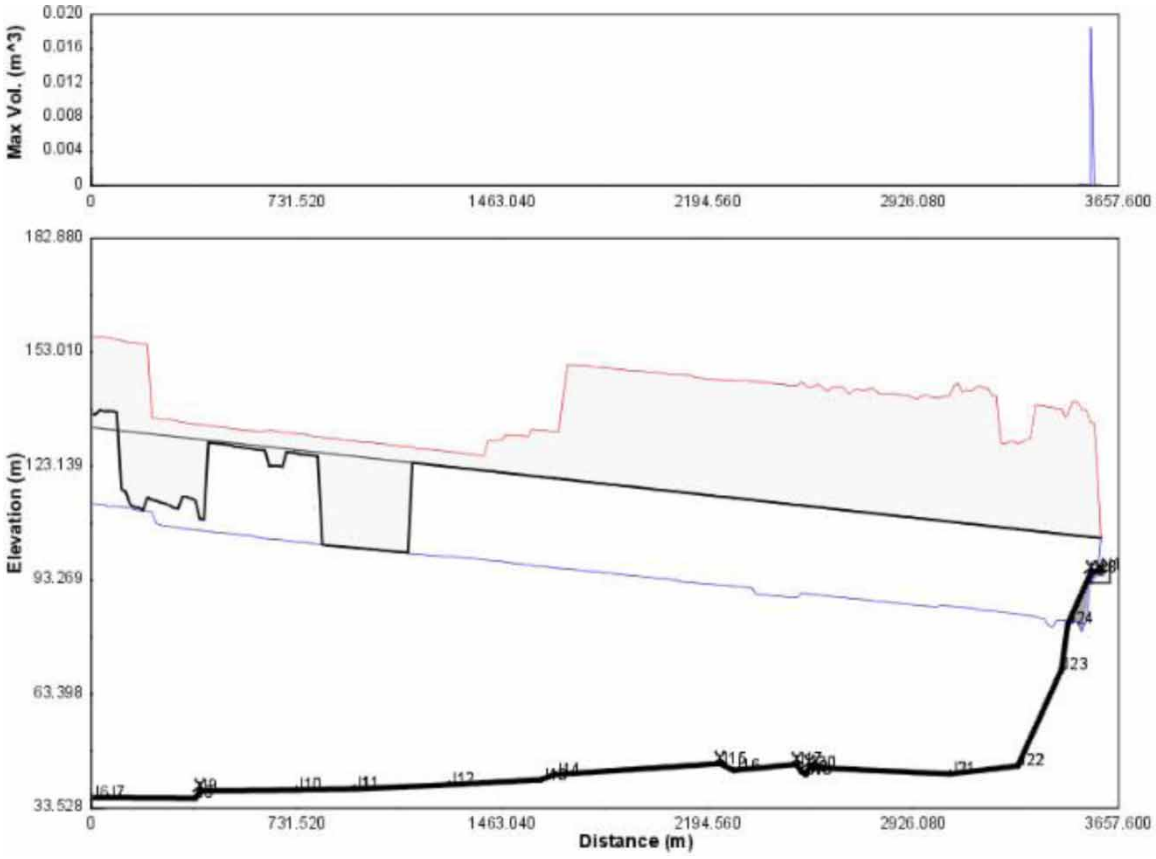

Figure 6 | Pressure variation (first record); Max. transient pressure (red line), Min. transient pressure (blue line), steady-state pressure variation (black line).

Table 4 | Test statistic and *p*-value calculation

Parameters	Surge velocity (m/s)	Air volume (%)
Chi-square	1.200	1.200
df	7	6
Asymp. sig.	0.991	0.977

In the present work, according to the Scatter diagram and curve fit (Figures 4 and 5) due to regression analysis for the velocity of surge or shock wave in a media with a free water bubble, the following equations would be valid:

$$a = \frac{1}{\left[\rho\left(\left(\frac{1}{k}\right) + \left(\frac{D}{E.t_w}\right) + \frac{n}{p}\right)\right]^{\frac{1}{2}}} \tag{26}$$

For the velocity of surge or shock wave with the high value of free water bubble the following equation would be valid:

$$a = \left(\frac{g.h}{n}\right)^{\frac{1}{2}} \tag{27}$$

In this work, the maximum amount of air infiltration which was calculated based on the achieved results was released by the air relief valve on the system. The air chamber prevented negative pressures and column

separation in the pipeline downstream of the pump station during power failure rundown. Flow into the chamber typically was designed to undergo a greater head loss than was experienced by an outflow. This situation damped the oscillatory flow over time. The sight glass showed the liquid surface in the chamber. Water level sensors determined when to turn the compressed air flow on or off and when to signal a violation of the upper or lower emergency levels. Pressure variation records (Figure 6) showed the sudden pressure drop due to the leakage zone in the water transmission line (the location of P1: J3 up to the location of P3: J8).

The sudden pressure drop occurred for maximum transient pressure (red line in Figure 6), minimum transient pressure (blue line in Figure 6), and steady-state pressure variation (black line in Figure 6). Due to the analysis of flow variations at 5 seconds, for the transmission line equipped with the surge tank, the results showed the high water flow rate variation at the entrance and exit was dependent on flow variation at the water hammer. This analysis incorporated pressure variation of transient flow and is in compliance with GIS localized the leakage zone in (Figure 6) in the water transmission line (the location of P1: J3 up to the location of P3: J8). The detail of leakage location and detection process were itemized in the hydraulic model.

3.1. Comparison of present work results with other expert research

In this work, the significant factors are as follows:

- The ratio of local leakage affected the values of wave oscillations period for both scenarios of the present work (Zhou *et al.* 2013).
- The bubbles were sucked into the system and caused high surge wave velocity (Figure 5).
- The pressure wave velocity was recorded in low transient time (up to 5 milliseconds).
- The scatter diagram due to regression analysis showed the suitable correlation of surge velocity against sucked air into the transmission line (Figures 3 and 4).

The other experts' works based on the numerical and experimental, for the field of fluid-structure interaction (FSI) in 1D pressurized transient flow, showed the technical challenge in the scope of 1D FSI. They emphasized assuming the appropriate coupling between the different pipe degrees of freedom without ending up in expensive computations. They showed, both numerically and experimentally, that FSI may generate overpressures higher than ones estimated by the classical solutions. Moreover, no engineering code or standard specifies when FSI has to be considered. All of these factors pinpoint that the physics of the FSI phenomena are not fully understood in common engineering practices and this involves the potential risk of underrated designs (Zhou *et al.* 2013). The present work based on the numerically and experimentally methods showed that regression analysis incorporated with the IoT and RS may generate higher precision through investigation of suitable data correlation for surge velocity against the volume of sucked air into the transmission line than those estimated by the classical solutions.

4. CONCLUSIONS

This work aimed to improve the advanced techniques for the safety of water transmission in the field of sub-atmospheric transient pressures. Hence, the maximum pressure and wave velocity due to the water hammer in the water transmission line were calculated based on the GIS. According to the GIS, the relationship classes between the spatial data and non-spatial data were defined for the scaled model. In the field test process, the spatial data and non-spatial data were collected and transmitted to PLC. The PLC was used as a tool for spatial data intercommunication of water system elements for water hammer investigation. The water hammer caused pressure variation, pipe breaks, and air entrance to the water pipeline. To reduce the penetrated air and repeated pipe breaks, the hydraulic model for analysis of water loss was defined in compliance with GIS based on the ArcGIS-ArcMap and HAMMER software. The Courant number calculated by HAMMER software was equal to 0.977 and the surge velocity was 1084 m/s. The pressure surge was detected by the RS facility equipped with sensors, advanced modems, and data loggers in 0.005 s referring to the IoT technique. The result of this work led to reducing the NRW and saving drinking water.

This work also led to raising the following suggestions for future research to improve modeling for the evaluation of pressure variation in water transmission line due to the water hammer:

- Make the connection between GIS, RS, and IoT for rapid data intercommunication to record the water pressure wave in a short time up to 1 second (in this work 0.005 s).
- Conceptual modeling definition for prediction of the pressure wave variation due to water hammer.

- Improvement of RS facilities installation equipped with data loggers, IoT and GEO-database intercommunication process.
- Relationship class definition for water system elements according to the type of connections (simple or complex) to apply the advanced method for accessing the leakage points in the calibration process of the transmission line.

ACKNOWLEDGEMENTS

The authors thank all specialists for their valuable observations and advice, and the referees for recommendations that improved the quality of this paper.

DATA AVAILABILITY STATEMENT

Data cannot be made publicly available; readers should contact the corresponding author for details.

CONFLICT OF INTEREST

The authors declare there is no conflict.

REFERENCES

Andrade, D. M. & de Freitas Rachid, F. B. 2022 A versatile friction model for Newtonian liquids flowing under unsteady regimes in pipes. *Meccanica; An International Journal of Theoretical and Applied Mechanics AIMETA* **57**, 43–72. https://doi.org/10.1007/s11012-021-01458-5.

Asli, K. H., Naghiyev, F. B. O., Haghi, R. K. & Asli, H. H. 2012 *Advances in Control and Automation of Water Systems*. Apple Academic Press. Taylor & Francis Group, New York, USA. https://doi.org/10.1201/b13114.

Asli, K. H., Aliyev, S. A. O., Thomas, S. & Deepu, A. 2017 *Handbook of Research for Fluid and Solid Mechanics: Theory, Simulation, and Experiment*. Apple Academic Press. Taylor & Francis Group, New York, USA. https://doi.org/10.1201/9781315365701.

Duan, H. F., Pan, B., Wang, M., Chen, L., Zheng, F. & Zhang, Y. 2020 State-of-the-art review on the transient flow modeling and utilization for urban water supply system (UWSS) management. *Journal of Water Supply: Research and Technology* **69**, 858–893. https://doi.org/10.2166/aqua.2020.048.

Ferras, D., Manso, A. P. A., Schleiss, A. J. & Covas, D. I. C. 2018 One-dimensional fluid-structure interaction models in pressurized fluid-filled pipes: a review. *Applied Science* **8**(10), 1844–1856. https://doi.org/10.3390/app8101844.

Hariri Asli, H. 2022 Investigation of the factors affecting pedestrian accidents in urban roundabouts. *Computational Research Progress in Applied Science & Engineering (CRPASE)* **8**(1), 1–4. Article ID: 2255. Available from: https://crpase.com/archive/CRPASE-Vol-08-issue-01-15172135.pdf, https://doi.org/10.52547/crpase.8.1.2255.

Hariri Asli, H. & Hozori, A. 2021 Non-Revenue Water (NRW) and 3d hierarchical model for landslide. *Larhyss Journal* **48**, 189–210. Available from: http://larhyss.net/ojs/index.php/larhyss/article/view/810/810.

Hariri Asli, H. & Nazari, S. 2021 Water age and leakage in reservoirs: some computational aspects and practical hints. *Larhyss Journal* **48**, 151–167. Available from: http://larhyss.net/ojs/index.php/larhyss/article/view/808/807.

Lema, M., Peña, F. L., Buchlin, J. M., Rambaud, P. & Steelant, J. 2016 Analysis of fluid hammer occurrence with phase change and column separation due to fast valve opening by means of flow visualization. *Experimental Thermal and Fluid Science* **79**(4), 143–153. doi:10.1016/j.expthermflusci.2016.07.008.

Möller, G., Detert, M. & Boes, R. M. 2015 Vortex-induced air entrainment rates at intakes. *Journal of Hydraulic Engineering* **141**(11). doi:10.1061/(ASCE)HY.1943-7900.0001036.

Sarkardeh, H., Zarrati, A. R., Jabbari, E. & Marosi, M. 2014 Numerical simulation and analysis of flow in a reservoir in the presence of vortex. *Engineering Applications of Computational Fluid Mechanics* **8**(4), 598–608. doi:10.1080/19942060.2014.11083310.

Vardy, A. E., Brown, J. M. B., He, S., Ariyaratne, C. & Gorji, S. 2015 Applicability of frozen-viscosity models of unsteady wall shear stress. *Journal of Hydraulic Engineering* **141**(1), 1–13. https://doi.org/10.1061/(ASCE)HY.1943-7900.0000930.

Zecchin, A. C., Maier, H. R., Simpson, A. R., Leonard, M. & Nixon, J. B. 2005 Parametric study for an ant algorithm applied to water distribution system optimization. *IEEE Transitions on Evolutionary Computation* **9**(2), 175–191. doi:10.1109/TEVC.2005.844168.

Zhao, L., Yang, Y., Wang, T., Han, W., Wu, R., Wang, P., Wang, Q. & Zhou, L. 2020 An experimental study on the water hammer with cavity collapse under multiple interruptions. *Water* **12**(9). https://doi.org/10.3390/w12092566.

Zhou, L., Liu, D. & Karney, B. 2013 Investigation on hydraulic transients of two entrapped air pockets in a water pipeline. *Journal of Hydraulic Engineering* **139**(9). doi:10.1061/(ASCE)HY.1943-7900.0000750.

First received 5 August 2022; accepted in revised form 26 September 2022. Available online 5 October 2022